SAE INTERNATIONAL™

CFD Modeling of Advanced Swirl Technique at Inlet-Runner for Diesel Engine

2015-26-0095
Published 01/14/2015

Bhagyada Dhingra
Vellore Institute of Technology

Sparsh Sharma
Moscow Institute of Physics & Technology

Kamalkishore Vora
ARAI

B Ashok
Vellore Institute of Technology

CITATION: Dhingra, B., Sharma, S., Vora, K., and Ashok, B., "CFD Modeling of Advanced Swirl Technique at Inlet-Runner for Diesel Engine," SAE Technical Paper 2015-26-0095, 2015, doi:10.4271/2015-26-0095.

Abstract

This paper summarizes the research work incorporated in the exploration of the potential of swirling in CI Engine and designing of a new mechanism, particularly at inlet, to deliver it to improve the in-cylinder air characteristics to eventually improve mixing and combustion process to improve the engine performance.

The research is concentrated on the measures to be done on engine geometry so as to not only deliver advantage to any specific fuel. According to the CI combustion theory, better engine performance may be achieved with Higher Viscous Fuel by improving the in-cylinder air-fuel mixing by increasing the swirl (rotation of air view from top of the cylinder) and tumble (rotation of air view from front of the cylinder) of in-cylinder air inside the fuel-injected region. The proposed inlet component is embedded with airfoil and is suitably designed after being iterated from four steps. The deciding factors of shape and orientation of these airfoils are height, chord length and number of blades. The preliminary assessment of the proposed component is performed on a CFD code using incompressible Navier-stokes with k-epsilon turbulence modeling. The 3D cold flow IC engine simulation is conducted on COSMOS and ANSYS Fluent. The validation of the results of in-cylinder airflow characteristics from simulations are compared with other related research works.

This paper is the first in series of our research on Diesel Engine. The experimental validation of the proposed component is currently going-on and would be presented in the next publication. The results show that the better mixing of fuel is achieved and the concentration of CO and Unburned Hydrocarbons is also reduced.

Introduction

The rate of depletion of petroleum based fuel due automobiles is now driving the current generation of engineers and scientists to develop new techniques of extracting power from the fuel and enhancing the overall efficiency of existing techniques. Currently, the world has a huge number of automobiles on the road using Internal Combustion Engine (IC Engine). It is estimated by World Energy Forum in 2009 that the worldwide reserves of crude oil will be exhausted in less than 100 years [1]. Compression Ignition (CI) engines, more commonly known as diesel engines, can operate on conventional petroleum diesel fuel but also on neat vegetable oil [2,3], non-edible oil [4, 5, 6, 7], waste cooking oil [8] and biodiesel [9]. Moreover a CI engine can be operated on biodiesel [10], hence, biodiesel can be a potential alternative fuel to replace or supplement depleted crude oil. Many attempts had been made by researchers to utilize this advantage. Among them, Celikten et al [11] compared CI engine performance fuelled with diesel, rapeseed and soybean fuels. Bio-diesel experiences a reduction of maximum power and torque of 1.0 kW and 2.1 N.m respectively compared to diesel [11]. Additionally the fuel consumption of rapeseed and soybean were also reported to increase from diesel by about 29 g/kWh and 47 g/kWh, respectively. These problems are mainly due to the inferior chemical properties of biodiesel compared to the conventional diesel fuel. The viscosity and density of biodiesel were reported to be higher and volatility lower than diesel fuel [12,13,14] which lead to the incomplete combustion and this eventually produces lower engine performance and affects the durability of the engine [15,16]. Furthermore the emission of toxic gases like CO, HC, aldehydes, particles and black smokes are also reported to be lower, in comparison to burning diesel fuel, except NOX, which is higher. The researches in this area are focused to

improve the properties of biodiesel by using additives [17], pre-heating the fuel to level its viscosity to that of diesel [18] and adjusting the injection timing [19].

The current research is focused on the measures to be done on engine geometry so as to not only deliver advantage to any specific fuel. The most popular techniques employed to improve the combustion efficiency using HVF (Higher Viscous Fuel due to their higher viscosity compared to petroleum diesel fuel) are preheating HVF before injection [8, 20] and changing the injection timing [21]. According to the CI combustion theory, better engine performance may be achieved with HVF by improving the in-cylinder air-fuel mixing by increasing the swirl (rotation of air view from top of the cylinder) and tumble (rotation of air view from front of the cylinder) of in-cylinder air inside the fuel-injected region. Various methods have been used to improve the in-cylinder airflow in diesel engines such as: closing part of the intake port using a butterfly valve [22,23,24,25] modifying intake port/manifold geometry inserting shroud around the intake valve and modifying the piston bowl. Alternatively, in-cylinder airflow may be improved through the use of a guide vane.

One of the primary approaches to get the fuel entirely oxidized is to make it mix properly with the air is swirling or commonly known as turbulence. The more is the swirling of air-fuel mixture, the more breakdown of viscous fuel particle is. The breakdown of these heavy fuel particles occurs during the compression/combustion stroke. The concept of organized air flow is not new and was first found for carbureted engine using gasoline using gasoline by using rotating blades placed between carburetor and intake manifold to provide more air swirl for efficient air-fuel mixing [26]. Afterwards, atomizers and fuel molecule breaker were patented with different identities [14].

Instead of duplicating what has been done, this research explores the potential of swirling in CI Engine and designing of a new mechanism to deliver it to improve the in-cylinder air characteristics to eventually improve mixing and combustion process to improve the engine performance. The figure shown below shows the basic shape of airfoils which has been tested in present work.

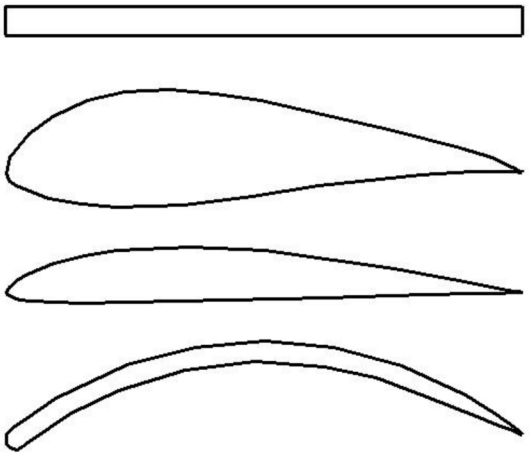

Figure 1. Different types of airfoil shortlisted for analysis

Swirl Generation during Induction

There are two broad tactics to create swirl during the induction stroke. In one, the flow is discharged tangentially toward the cylinder wall, where it is deflected sideways and downward in a swirling motion. In the other, the swirl is largely generated within the inlet port: the flow is forced to rotate about the valve axis before it enters the cylinder.

Governing Equations: COLD Flow Analysis

The three major equations used in the computational fluid dynamics problem are Continuity equation, Momentum equation (Navier-stokes equation) and Energy equation. For the generalized fluid flow problems mostly two equations are used. The first one is Continuity equation which fulfils the law of conservation of mass, thus a mass balance requirement posed in a mathematical form and the second one is Navier-stokes equation which fulfils the law of conservation of momentum. The Navier-stokes equations are vector hence they have separate set of equations for each coordinate direction. On the basis of control volume, the continuity equation is derived as follows:

$$\frac{\partial \rho}{\partial t} + \nabla.(\rho U) = 0 \tag{1}$$

Where ρ is the fluid density and U is the three dimensional flow velocities in x, y and z directions. The Navier-stokes equation is based on the Newton's second law where the forces taken into account are body forces and surface forces on the control volume and is derived as follows:

$$\frac{\partial (\rho U)}{\partial t} + \nabla.(\rho U \times U) = -\nabla p + \nabla.\tau + S_M \tag{2}$$

In this equation p, τ and S_M are the fluid pressure, strain rate and momentum source, respectively. Since this problem is quite a complex thus the involvement of Energy equation in the calculations is inevitable. The rate of change of energy inside the fluid element which is equal to the combined net flux of heat into the element and the net rate of work done on the element due to the body and surface forces comprises the Energy equation which is further mathematically denoted as follows:

$$\frac{\partial (\rho h_{tot})}{\partial t} - \frac{\partial \rho}{\partial t} + \nabla.(\rho U h_{tot}) = \nabla.(\lambda \nabla T) + \nabla.(U.\tau) + U.S_M \tag{3}$$

Where h_{tot} and λ represent the total enthalpy and thermal conductivity respectively of the fluid.

The engine simulation model is modelled conferring to the Kirloskar TAF-1 diesel engine coupled with a generator that operated at a constant speed of 1500 rpm. The technical specifications of the engine are listed in Table 2. SolidWorks 2014 is used to model the

essential drawings of the intake port, intake runner, intake valve, and cylinder volume. The dynamic analysis is carried out in ANSYS Fluent. The CFD simulation is carried out for only cold flow without combustion. At the boundaries i.e. at the intake as well as exhaust manifold, constant pressure conditions are given. Logarithmic law of wall unified with No-slip wall boundary condition is used. Moreover the simulation is dynamic and time dependent thus turbulence modeling comes into play.

Turbulence Modeling of the Swirling Flow

The swirl number is mathematically defined as follows:

$$SW = \frac{\int r v_\theta (\vec{v}.\hat{n}) dS}{\bar{r} \int v_z (\vec{v}.\hat{n}) dS} \quad (4)$$

where r is the radial coordinate (specifically, the radial distance from the axis of rotation), vΘ is the tangential velocity, $\vec{v}$ is the velocity vector, $\hat{n}$ a unit vector normal to the surface, S is the inlet or outlet.

For flows with weak to moderate swirl (S < 0.5), both the RNG ***k - ϵ*** model and the realizable ***k - ϵ*** model yield appreciable improvements over the standard ***k - ϵ*** model. For highly swirling flows (S > 0.5), the RNG ***k - ϵ*** model is strongly recommended. The effects of strong turbulence anisotropy can be modeled rigorously only by the second-moment closure adopted in the RNG ***k - ϵ*** model

In this study RNG k-ε model is used. “k” is the turbulence kinetic energy and is defined as the variance of the fluctuations in velocity and “ε” is the turbulence eddy dissipation and has dimensions of k per unit time. The TKE equation after few simplifications is as follows:

$$\frac{\partial k}{\partial t} + u_j \frac{\partial k}{\partial x_j} = \tau_{tij} \frac{\partial u_i}{\partial x_j} - \varepsilon + \frac{\partial}{\partial x_j}\left[V + {}^{v_t}/_{\sigma_k} \frac{\partial k}{\partial x_j}\right] \quad (5)$$

$$\tau_{t,ij} = -\overline{u_i u_j} = 2 v_t S_{ij} - \frac{2}{3} k \delta_{ij} \quad (6)$$

The first term on the RHS is the production of ‘k’, the second term (ε) is the specific dissipation per unit mass. The last terms describe the transport of ‘k’ by molecular and turbulent diffusion. This model is best suited for flows with high Reynolds number where turbulence is almost isotropic. The scale elimination procedure in RNG theory results in a differential equation for turbulent viscosity:

$$d\left(\frac{\rho^2 k}{\sqrt{\varepsilon \mu}}\right) = 1.72 \frac{\hat{\nu}}{\sqrt{\hat{\nu}^3 - 1 + C_\nu}} d\hat{\nu} \quad (7)$$

$$\hat{\nu} = \mu_{eff}/\mu$$

$$C_\nu \approx 100$$

The problem here is axisymmetric with respect to geometry and flow conditions and includes swirl or rotation. In this case, the flow can be modelled as 2D for initial purpose so as to save the time (i.e., solve the axisymmetric problem) and include the prediction of the circumferential (or swirl) velocity. It is important to note that while the assumption of axisymmetric implies that there are no circumferential gradients in the flow, there may still be non-zero swirl velocities as shown in the figure:

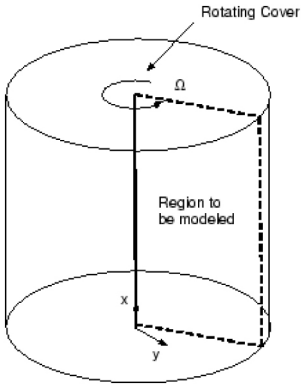

Figure 2. In-cylinder picture showing the region needed to be modeled

Dynamic Meshing for Piston Movement

The to and fro motion of piston is modeled using the technique known as Dynamic mesh. It allows the movement of the boundaries of a cell zone relative to other boundaries of the zone, and to adjust the mesh accordingly. The boundaries can move rigidly with respect to each other (i.e., linear or rotational motion), and/or deform. The relative motion of stationary (cylinder) and moving (piston) components gives rise to transient interactions.

Mesh Update Method

As per the availability of mesh motion methods in ANSYS Fluent, Spring-Based Smoothing and Dynamic Layering Method are chosen which are further explained in subsequent section.

Spring-Based Smoothing

In the spring-based smoothing method, the edges between any two mesh nodes are idealized as a network of interconnected springs. The initial spacing's of the edges before any boundary motion constitute the equilibrium state of the mesh. A displacement at a given boundary node will generate a force proportional to the displacement along all the springs connected to the node. Using Hooke's Law, the force on a mesh node can be written as [45]:

$$\vec{F_i} = \sum_j^{n_i} k_{ij} \left(\Delta\overline{x_j} - \Delta\overline{x_i}\right) \quad (8)$$

where $\Delta\overline{x_i}$ and $\Delta\overline{x_j}$ are the displacements of node *i* and its neighbor *j*, n_i is the number of neighboring nodes connected to node *i*, and k_{ij} is the spring constant (or stiffness) between node *i* and its neighbor *j*. The spring constant for the edge connecting nodes *i* and *j* is defined as

$$k_{ij} = \frac{1}{\sqrt{|\overline{x_i} - \overline{x_j}|}} \quad (9)$$

Dynamic Layering Method

In prismatic mesh zones, dynamic layering method adds or removes layers of cells adjacent to a moving boundary, based on the height of the layer adjacent to the moving surface. The dynamic mesh model in ANSYS FLUENT allows you to specify an ideal layer height on each moving boundary.

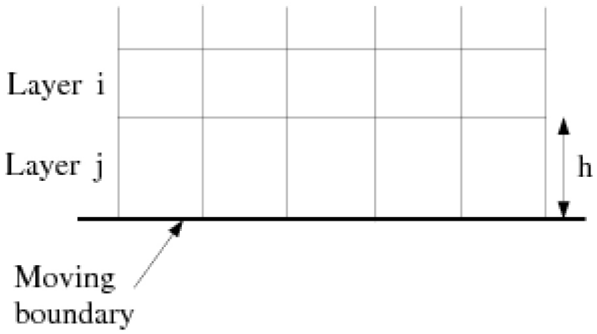

Figure 3. Dynamic layering at the moving boundary layer (piston-cylinder wall)

If the cells in layer j are expanding, the cell heights are allowed to increase until

$$h_{min} > (1 + a_s)h_{ideal} \quad (10)$$

Here h_{min} is the minimum cell height of cell layer j, h_{ideal} is the ideal cell height, and a_s is the layer split factor.

If the cells in layer j are being compressed, they can be compressed until

$$h_{min} < a_c h_{ideal} \quad (11)$$

where a_c is the layer collapse factor. When this condition is met, the compressed layer of cells is merged into the layer of cells above the compressed layer; i.e., the cells in layer j are merged with those in layer i.

Implicit Update Settings

For such applications, having the mesh motion updated within the time step based on the converging flow solution results in a stronger coupling between the flow solution and the mesh motion, and leads to a more robust solver run. Implicit mesh updating allows you to run simulations that otherwise could not be solved or would require an unreasonably small time step. The relaxation of the displacements is defined by the following equation [45]:

$$x_k = \omega\left(x_{computed,k}\right) + (1 - \omega)x_{k-1} \quad (12)$$

Where x_k is the node position at iteration k (within a time step), $x_{computed,k}$ is the computed node position (based on the flow field), and ω is the motion relaxation.

The simulation goes projected when the geometry gets the required set of physical parameters associated with the operational conditions. In preceding sections, it is decided to go with k-ϵ Turbulence modelling with dynamic meshing supported by spring based smoothing and dynamic layering.

Boundary Conditions

This section describes the associated boundary conditions with the suction stroke in CI engine. There is no turbocharging linked with the in-take stroke. The following figure shows all the attached boundary conditions to every important component.

The simulation goes projected when the geometry gets the required set of physical parameters associated with the operational conditions. In preceding sections, it is decided to go with k-ϵ Turbulence modeling with dynamic meshing supported by spring based smoothing and dynamic layering.

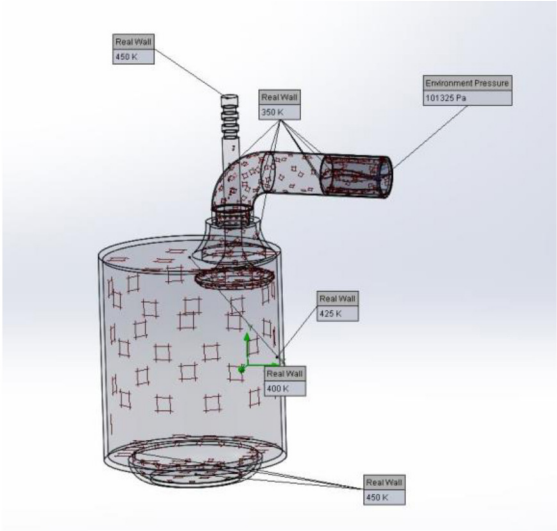

Figure 4. Engine geometry showing all the boundary conditions attached

The following table.1 tabulates all the boundary conditions attached to its respective component.

Table 1. Boundary conditions attached to their significant component

Component	Boundary Condition
Opening of inlet runner	P=101325 Pa; T= 300K (Environmental pressure)
Inlet runner pipe	T=350K (Real wall)
Valve	T=450K (Real wall)
Top surface of the cylinder	T=400K (Real wall)
In-cylinder wall	T=425K (Real wall)
Bottom of the cylinder and top of the piston	T=450K (Real wall)

Simulation Results and Discussion

A complete parametric study of four different types of blade shape incorporated in the component is done computationally in this chapter. Parametric study is performed with the component maintaining the constant engine geometry throughout the analysis for four different configurations namely S1 to S4.

The method of testing adopted for this project is one of learning from the results of each shape tested, and implementing appropriate changes in the subsequent blade shape. The best configuration is then chosen after analyzing computational result and comparing various plots for in-cylinder velocity and vorticity.

As for preparing the simulation model, SolidWorks 2014 was utilized to draw the four different blade shape design and S1 to S4 configuration for Advanced Swirl Device (ASD). The best design is then chosen by comparing the results obtained by CFD analysis.

The for k-ϵ turbulence modeling brought the following plots. It can be construed from the figure shown below that the velocity of the fluid at the cylinder wall is apparently negligible as compared to the velocity in the core of cylinder. This evidences the problem of formation of thin wall of charge inside the cylinder in CI engine.

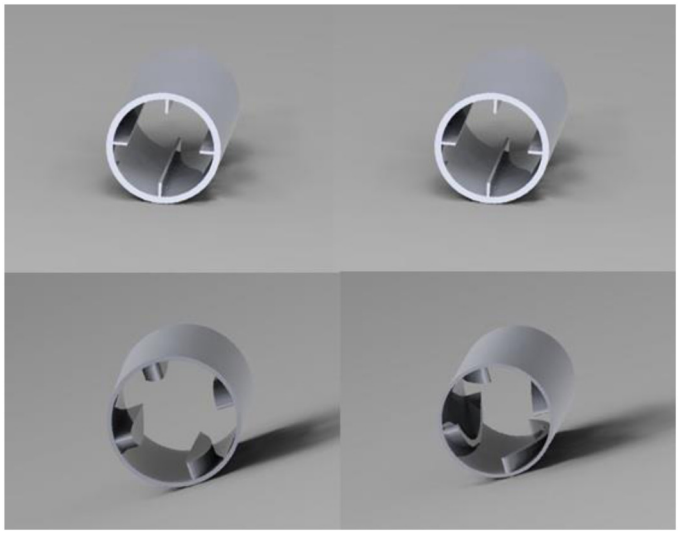

Figure 5. ASD-S1 to S4 (from left to right)

Additionally, vorticity plot also shows a level of turbulence (disturbance) directly beneath the port which fades out when moving away from the axis in radial direction. The blue color depicts the zero magnitude of swirl parallel to the cylinder head plane as shown in figure.6.

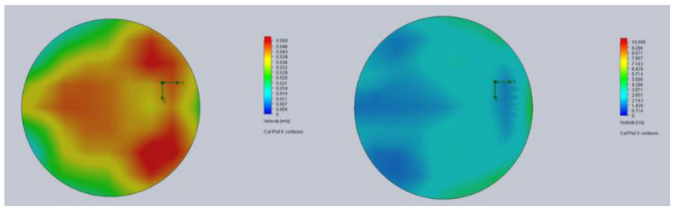

Figure 6. Cut plot showing velocity (left) and vorticity (right) distribution in baseline configuration

In the figure.7, a comparison of velocity among all the proposed ASDs is shown. The in-cylinder velocity in S1 and S3 is relatively less when compared with that of S2 and S4. The more the green color a plot has the less the swirl it has and adhering to which configurations S1 and S3 simply draw out from the further comparison. Now moving towards the left ones, S4 delivers high in-cylinder velocity at almost every point.

Nevertheless S4 has a static region in the right side of the cylinder, S2 has certainly very low velocity in the core of the cylinder.

Next illustration (figure.8) shows the vorticity cut plot. The circular motion along the vertical axis or simply swirl is inferred from this plot. Configuration S1 delivers mixed response whereas S2 and S4, as expected, distribute more swirl inside the cylinder. Performance of S3 is dramatically poor in this context, the flow remain irrotational all the time. The more the rotational flow near the walls, the less the formation of fluid film there; S4 has more vorticity vectors at every visible location inside the cylinder as compared to others.

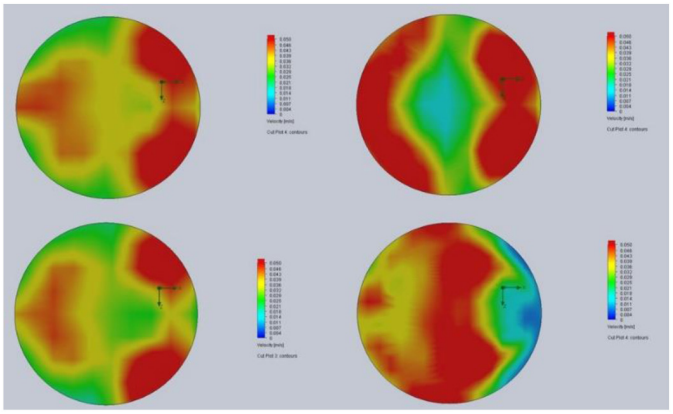

Figure 7. Cut plot showing velocity distribution in S1-S4 (clockwise from top left) configurations

Adding up the results from all the cut plots, it is inferred that S2 and S4 are the best possible designs for ASD, but to move on for further iteration process it is suggested to select the best so that advance design changes can be introduced into the selected design. A thorough analysis of the plots suggest a draw between S2 and S4 whereas figure 7 and 8 characterize the drawbacks in S2 thus marking S4 as the best suited ASD design.

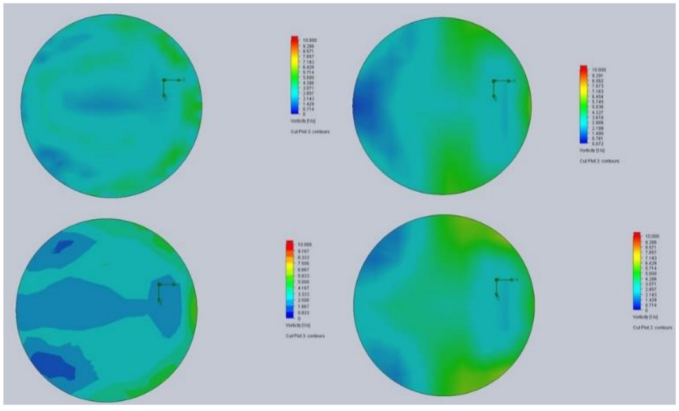

Figure 8. Cut plot showing vorticity distribution in S1-S4 (clockwise from top left) configurations

The overhead discussion simply suggest that configuration S4 is best among all the proposed designs, thus the usage of a cambered airfoil in the inlet runner can be considered fruitful in terms of increasing in-cylinder velocity and swirl resulting in less emission.

Since this is a progressive iteration process, S4 moves on the next iteration process and will be tested with next design optimization.

After being decided upon the shape, the designing process of ASD arrives at phase-2. The positioning of the device is considered the second important parameter. Parametric study is carried out with the component placed at two different positions namely L1 and L2 as shown in figure.9.

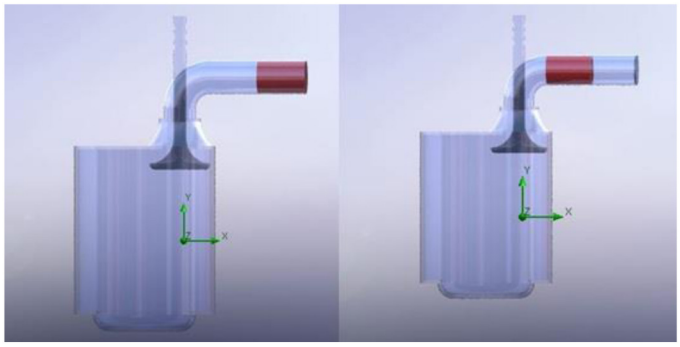

Figure 9. ASD-L1 (left) and ASD-L2 (right)

The cut plot shown in figure.10 shows the difference between velocity distributions inside the cylinder delivered by L1 (left) and L2 (right). In configuration L1, the particle moves somewhat slower inside the cylinder, the yellow region near the ports and around the walls proves this.

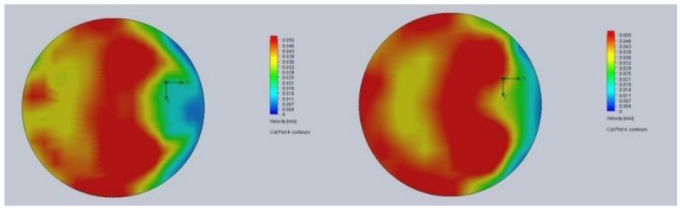

Figure 10. Cut plot showing velocity distribution in L1 (left) and L2 (right) configurations

Looking at L2 configuration, the red portion is more than any other color. The velocity near the axis of the cylinder is also very high in this case. On the right side of the cylinder, blue color is visible which shows the area of high tumble, this is caused due to usage of conventional valve in the analysis.

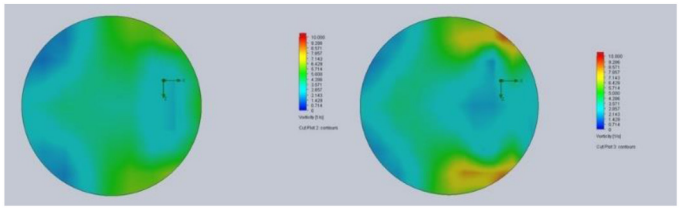

Figure 11. Cut plot showing vorticity distribution in L1 (left) and L2 (right) configurations

Figure.11 shows the vorticity plot for both the configurations. The swirl intensity is high in L2 configuration at every place. On the walls where velocity seems to less in previous graph, vorticity plot evidences the presence of high swirl at those positions. In L1 the swirl is critically less the left side of the cylinder whereas in L2 the red and yellow color confirms the high swirl.

From above interpretation, ASD-S4-L2 comes out to be the best and can be moved on the next the iteration phase.

Till now S4 shape with L2 positioning is confirmed by the robust computational analysis. This chapter deals with the optimization of the component for number of blades. A parametric study is performed with the component maintaining the constant engine geometry throughout the analysis. Three different ASDs with different number of blades have been modeled, in SoildWorks 2014, namely B1, B2, and B3.

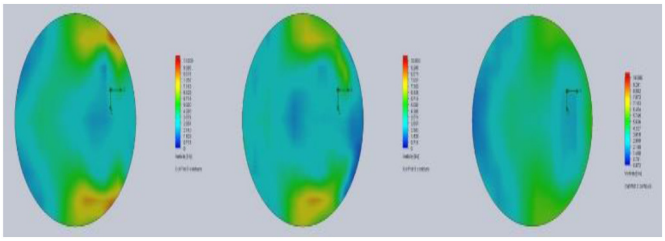

Figure 12. Cut plot showing velocity distribution in B1, B2, and B3 (from left to right)

The figure.12 illustrates the velocity distribution inside the cylinder. All the three configuration differ from each other. The plot on the extreme right (eight blade configuration) has almost zero velocity around the wall of the cylinder. The two red spots around the central axis show high velocity swirls in the center but due to the presence of more blue and green color it stands last in the comparison. Coming to the configuration B2 (six blades), the velocity around the wall on the right side is pretty low but in the core of cylinder the presence of more red color is quite an evidence of high velocity vectors

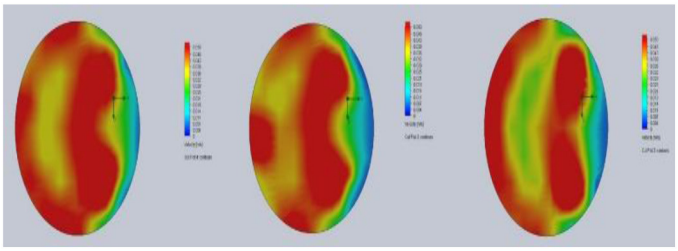

Figure 13. Cut plot showing vorticity distribution in B1, B2, and B3 (from left to right)

With the most of red color inside the cylinder, configuration with four blades can be considered as the best in terms of velocity distribution. The little yellow spot near the left wall shows some static region but overall it has better performance capabilities.

Now comes to the vorticity plot. This plot also favors the coin to B1. The high pressure swirl is present around the wall of B1. B2 also has good turbulence relative to B1. Upon looking B3, there is no sign of high swirl.

From above interpretation, ASD-S4-L2-B1 comes out to be the best and can be moved on the next the iteration phase.

This section is the last in this iteration process, counts the parametric study of three different configurations of ASD with four blades but of different heights namely H1, H2, and H3. The study is performed with components maintaining the constant engine geometry throughout the analysis.

The next plot is the velocity distribution inside the cylinder of all the three configurations having blades with different height as shown in figure.14. The picture in the extreme right is having blade of 4.5mm length. It is previously mentioned that these blades will impart obstruction to the air flow. Furthermore, the presence of more green and yellow color in H3 prove the presence of static dead fluid zone which is not good for combustion. Now coming to H2 (picture in the middle), the velocity vector is somewhat increased relatively H1, yet the presence of more yellow and red color in this configuration prove that increasing the length of blade is definitely increasing the obstruction to the incoming air. Now moving to H1 (extreme left) which has blade height of 2.5mm length. The velocity near the wall and around the central axis is comparatively high compared to every other configuration.

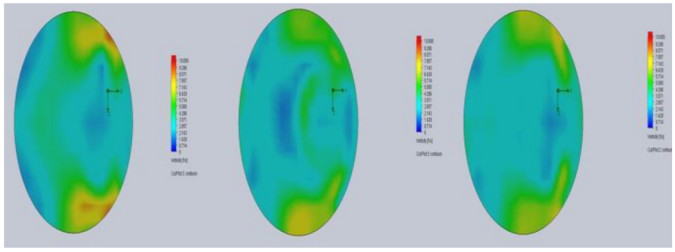

Figure 14. Cut plot showing vorticity distribution in H1, H2, and H3 (from left to right)

The final plot in the series of this long iteration process is the vorticity plot accommodating H1, H2, and H3 as shown in figure 15. Looking at the extreme right, H3 configuration, the vorticity around the wall is observed which diminishes when moving in to the central axis. Two dead zones are clearly visible. H2 delivers a surprisingly high vortical flow with yellow portion motivating the presence of swirls. Finally coming to H1, i.e. 2.5mm long blades, the vortical flow is strongest in this configuration with least concentration of dead fluid zones. The red portion on the right side of the cylinder wall is a great indication of high velocity swirl.

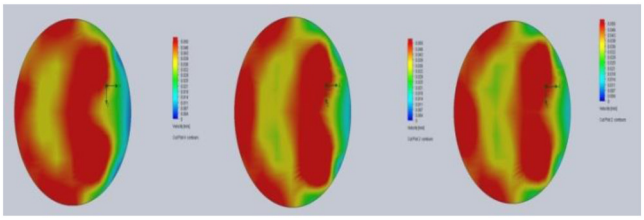

Figure 15. Cut plot showing vorticity distribution in H1, H2, and H3 (from left to right)

From above interpretation, ASD-S4-L2-B1-H1 comes out to be the best and can be moved on the next phase of this project which is prototyping and experimental tests on engine bed.

Experimental Results and Discussion

This section is certainly the most important chapter of this paper. It includes the prototyping of Advanced Swirl Device and its installation, commissioning and run of the engine. Substantial development of the engine test facility was necessary before testing could begin.

After being iterated in long designing process ASD has finally taken its shape. The CAD model is prepared in SolidWorks 2014 and has been scaled up for the purpose for being tested on the available facility. The manufacturing process incorporated in manufacturing ASD is also mentioned in this chapter.

The engine available at VIT University is a Kirloskar TAF-1 diesel engine used for agricultural application which is a constant speed of 1500 rpm. Full specification of this engine and installation of ASD at the inlet runner is elaborated in this chapter.

The final section deals with the results and validates the computational results obtained from CFD analysis.

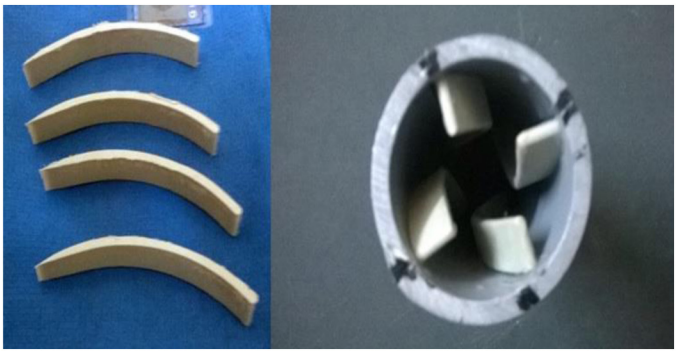

Figure 16. Manufactured blades (left) according to S4-B1-H1 configuration and the final ASD (right) with blades embedded inside the cylindrical pipe

The final ASD as shown in figure 16 has been manufactured using CNC

The engine simulation model is modelled conferring to the Kirloskar TAF-1 diesel engine that operated at a constant speed of 1500 rpm is coupled with a eddy current dynamometer. The technical specifications of the engine are listed in Table 2. SolidWorks 2014 is used to model the essential drawings of the intake port, intake runner, intake valve, and cylinder volume.

The analysis is done for 5 load variations namely 20%, 40%, 60%, 80%, and 100%; with and without ASD.

Figure 17. Kirloskar TAF-1 Diesel Engine

The engine test is made possible not only because of engine but also the auxiliaries like electronic display board which shows engine speed in rpm, data acquisition system recording every bit, fuel tank holding enough diesel fuel for the test, gas analyzer for analyzing the emission constituents, and dynamometer. Schematic diagram of the experimental set up is depicted in figure 18.

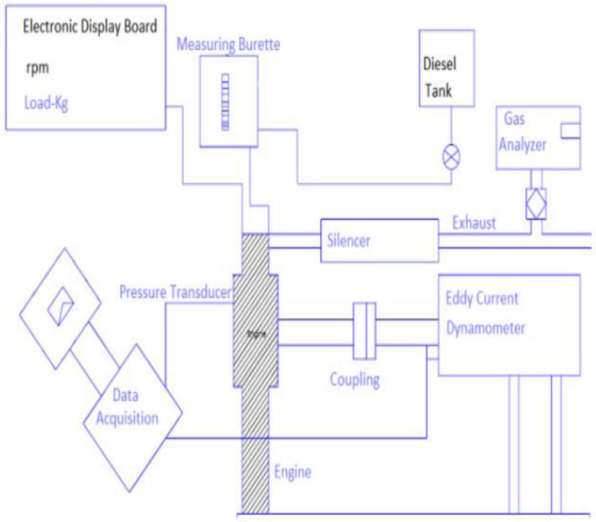

Figure 18. Overall experimental set-up

Table 2. Engine specifications

Parameter	Value
No. of Cylinders	1
Bore * Stroke	87.5 x 110mm
Cubic Capacity	0.662 ltr
Compression Ratio	17.5:1
Rated Output	4.41 KW
Rated Speed :	1500 rpm (Constant Speed)
Specific Fuel Capacity (SFC)	195 gm/hp-hr
Fuel Tank Capacity	6.5 ltr
Engine Weight (dry)	163 kg
Starting :	Hand start

The following table tabulates engine specifications in a broad way.

When the engine speed is kept constant, the performance of a diesel engine is mainly dictated by the quantities of diesel fuel injected. Usually, the specific fuel consumption decreases while the exhaust temperature increases with the increase in engine power, and NOx and CO2 emissions increase with the increased addition of the diesel fuel. The same phenomena is observed here but a variation in the concentration of CO2 and NOx in both the engine configuration is observed.

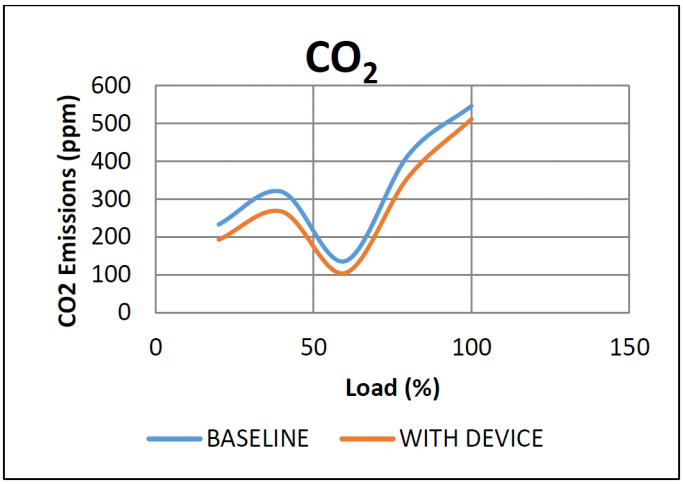

Figure 19. CO2 emissions vs load

Both the graphs show no deviation to each other. At 20% load the baseline engine run produces 233ppm CO2 whereas run with ASD produces only 193ppm which is 40ppm less CO2 emissions at minimal load. At 40% load, ASD engine run emits 50ppm less CO2. This trend is dominant for all the load values and on an average engine with ASD emits 45ppm less CO2 than an engine without ASD.

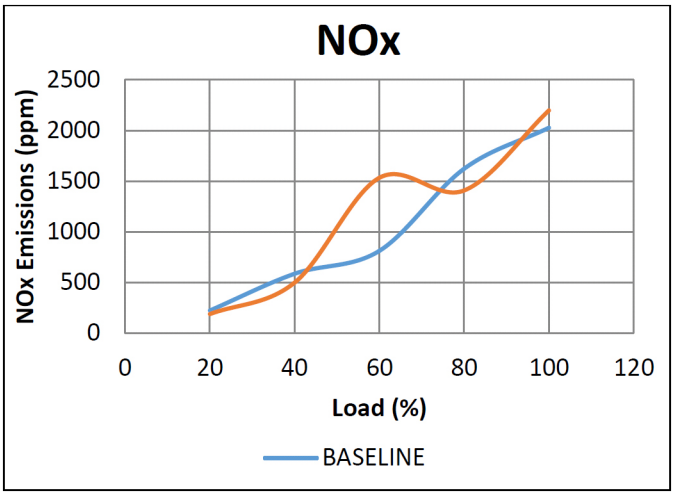

Figure 20. NOx emissions vs load

Since the NOx formation is more complex than any other pollutant so are its measures. At nominal load of 20%, instead of a drop in NOx emissions, an unexpected rise of 35ppm is observed which could be estimated due to more mixing inside the cylinder. At 40% load the emissions get lower in ASD engine whereas the baseline engine keep following the same trend. It can be simply inferred from the figure 20 that NOx emission increases in engine with ASD which could a possible outcome of more mixing. So it is advisable for future work if catalytic converter can be incorporated in the research work for further development of this new idea.

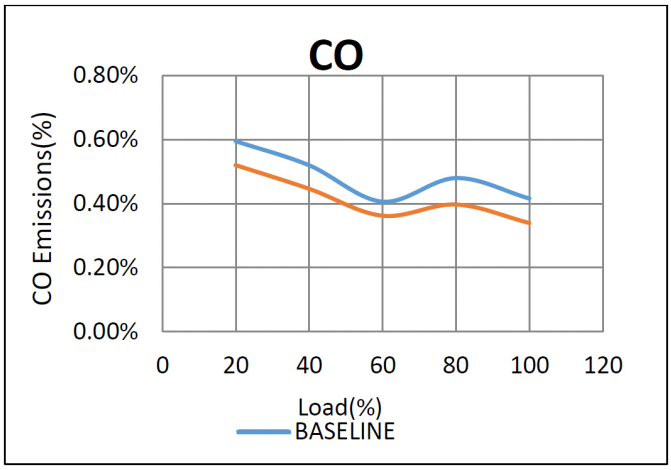

Figure 21. CO emissions vs load

The results obtained for CO and unburned hydrocarbons, the ASD seem advantageous. With the increment in load from 20% to full load condition reduction 0f 0.05% CO to 0.07% CO emissions are observed with the usage of ASD.

From initial load variation to the final load, a drop of HC emissions is observed in the range of 50 ppm to 200 ppm with the usage of ASD.

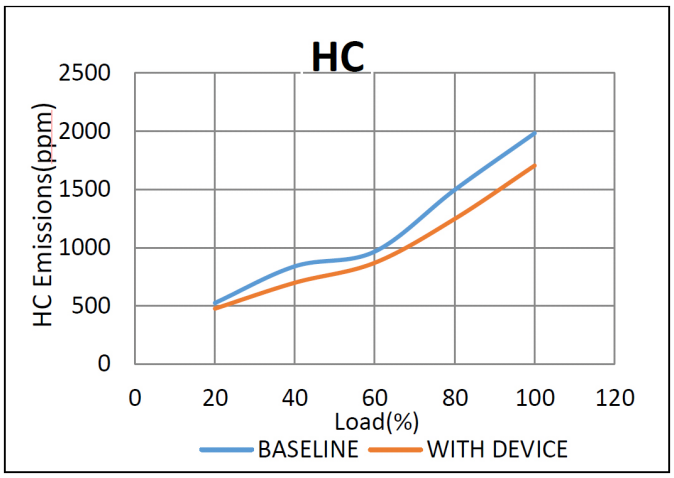

Figure 22. HC emissions vs load

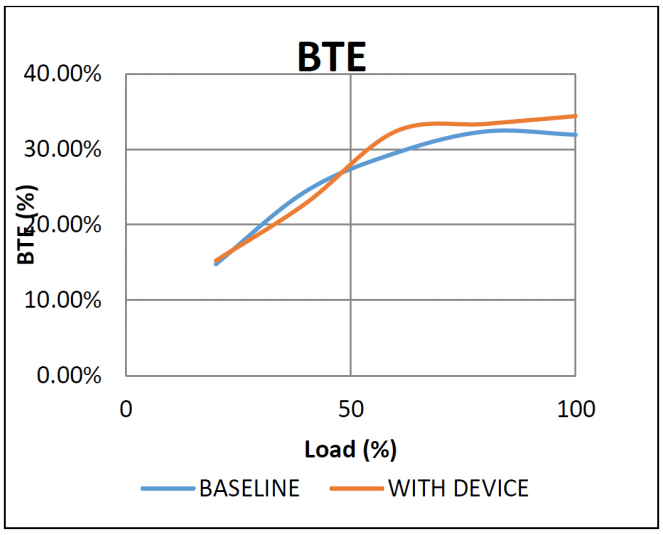

Figure 23. Brake Thermal Efficiency (BTE)

Concluding remark in favor of ASD is evidently given by this positive variation in BTE. At initial 20% load, there is no difference observed in efficiencies of both the configurations.

Till 50% load conditions, baseline performs better in terms of efficiency but after 50% the configuration with ASD topples up everything in favor of this new invention.an overall rise of 3.12% is calculated, which means using ASD increases the BTE by 3%.

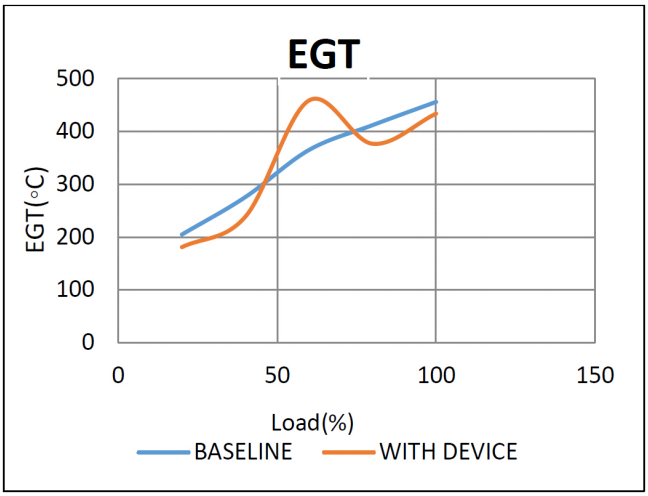

Figure 24. Exhaust Gas Temperature (EGT)

Certainly the reason for trivial performance of ASD for NOx emissions could be explained with the help of figure 24. A very oscillating data has been recorded for EGT. Between the intervals of 40% load to 75% load, engine with ASD produces higher temperature exhaust whereas the baseline engine shows a linear curve for all the ranges of loads. Beyond 80% load conditions, ASD lowers down the exhaust gas temperature by 5%.

Summary & Conclusions

Advanced Swirl Devices (ASDs) were tested by performing a rigorous design and analyses process consisting of both CFD simulations and experimental tests on an engine bed. This encompassed a wide range of boundary conditions, engine speeds and loads. And provided a suitable basis upon which to compare thee emissions performance of each ASD.

Substantial variances in the trend of CO2, NOx, CO and unburned Hydrocarbons between different mode tests.

The figure shown below depicts the advantage ASD is delivering in terms of enhancing swirl and mixing of fuel-air particles. The more red color is visible in ASD configuration which evidences more turbulence and swirl inside the chamber.

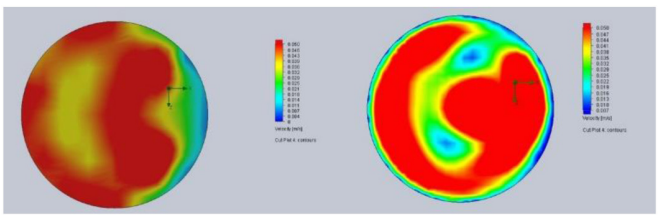

Figure 25. Cut plot showing velocity comparison between baseline (left) and ASD-S4-L2-B1-H1

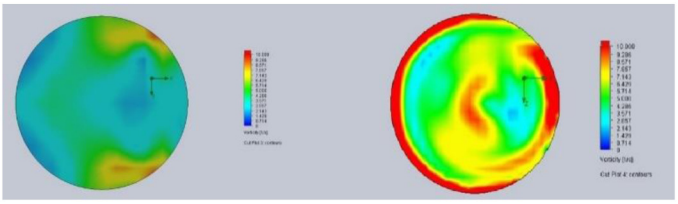

Figure 26. Cut plot showing vorticity comparison between baseline (left) and ASD-S4-L2-B1-H1

ASD-S4-L2-B1-H1 has been prototyped and is tested on the engine bed. The engine ran twice; one with the device and one without device. The fuel used is diesel without pre-heating. The exhaust gas analyzer analyzed the exhaust at every load and it is evidently recorded that the application of ASD at the inlet reduces CO2, CO, Unburned HCs. This is due to the proper mixing of air-fuel particles because as expected ASD has imparted high velocity vortical flow into the cylinder.

A drop in the range of 50-200 ppm is observed in HC emissions, furthermore a reduction of 0.05% CO is also observed. While moving towards CO2 a descent of 50ppm is achieved.

Brake thermal efficiency is surprisingly increased by 3% which needs to be validated with more robust engine tests in future.

References

1. Sharma, Y.C. and Singh B., Development of biodiesel: Current scenario. Renewable and Sustainable Energy Reviews, 2009. 13(6-7): p. 1646-1651.
2. Lim, S. and Lee K.T., Implementation of biofuels in Malaysian transportation sector towards sustainable development: A case study of international cooperation between Malaysia and Japan. Renewable and Sustainable Energy Reviews, 2012. 16(4): p. 1790-1800.
3. Bari, S., Yu C., and Lim T., Performance deterioration and durability issues while running a diesel engine with crude palm oil. Proceedings of the Institution of Mechanical Engineers, Part D: Journal of Automobile Engineering, 2002. 216(9): p. 785-792.
4. Russo, D., et al., State of the art of biofuels from pure plant oil. Renewable and Sustainable Energy Reviews, 2012. 16(6): p. 4056-4070.
5. Atabani, A.E., et al., A comprehensive review on biodiesel as an alternative energy resource and its characteristics. Renewable and Sustainable Energy Reviews, 2012. 16(4): p. 2070-2093.
6. Ayhan, D., Use of algae as biofuel sources. Energy Conversion and Management, 2010. 51(12): p. 2738-2749.
7. Demirbas, A. and Fatih Demirbas M., Importance of algae oil as a source of biodiesel. Energy Conversion and Management, 2011. 52(1): p. 163-170.
8. Bari, S., Lim T.H., and Yu C.W., Effects of preheating of crude palm oil (CPO) on injection system, performance and emission of a diesel engine. Renewable Energy, 2002. 27(3): p. 339-351.
9. Kumar, D.J. and Binnal P., Performance evaluation of a single cylinder diesel engine fueled with biodiesel produced from pumpkin oil. Journal of Scientific & Industrial Research, 2012. 71: p. 75-78.
10. Murugesan, A., et al., o as an alternative fuel for diesel engines-A review. Renewable and Sustainable Energy Reviews, 2009. 13(3): p. 653-662.
11. Çelikten, İ., Koca A., and Ali Arslan M., Comparison of performance and emissions of diesel fuel, rapeseed and soybean oil methyl esters injected at different pressures. Renewable Energy, 2010. 35(4): p. 814-820.
12. Agarwal, A.K., (2007). Biofuels (alcohols and biodiesel) applications as fuels for internal combustion engines. Progress in Energy and Combustion Science 33(3), 233-271.
13. Candeia, R.A., Silva, M.C.D., Carvalho Filho, J.R., Brasilino, M.G.A., Bicudo, T.C., Santos, I.M.G., Souza, A.G., (2009). Influence of soybean biodiesel content on basic properties of biodiesel-diesel blends. Fuel 88(4), 738-743.
14. Jaichandar, S., Annamalai, K., Effects of open combustion chamber geometries on the performance of pongamia biodiesel in a DI diesel engine. Fuel (0).
15. Bari, S., (2004). Investigation into the deteriorated performance of diesel engine after prolonged use of vegetable oil, ASME 2004 Internal Combustion Engine Division Fall Technical Conference ASME, Long Beach, California, USA.
16. Bari, S., Yu, C., Lim, T., (2002b). Filter clogging and power loss issues while running a diesel engine with waste cooking oil. Proceedings of the Institution of Mechanical Engineers, Part D: Journal of Automobile Engineering 216(12), 993-1001.
17. Moser, B.R., (2008). Influence of Blending Canola, Palm, Soybean, and Sunflower Oil Methyl Esters on Fuel Properties of Biodiesel†. Energy & Fuels 22(6), 4301-4306.
18. Pugazhvadivu, M., Jeyachandran, K., (2005). Investigations on the performance and exhaust emissions of a diesel engine using preheated waste frying oil as fuel. Renewable Energy 30(14), 2189-2202.
19. Ye, P., Boehman, A.L., (2012). An investigation of the impact of injection strategy and biodiesel on engine NOx and particulate matter emissions with a common-rail turbocharged DI diesel engine. Fuel 97(0), 476-488.
20. Agarwal, D. and Agarwal A.K., Performance and emissions characteristics of Jatropha oil (preheated and blends) in a direct injection compression ignition engine. Applied Thermal Engineering, 2007. 27(13): p. 2314-2323.
21. Bari, S., Yu C., and Lim T., Effect of fuel injection timing with waste cooking oil as a fuel in a direct injection diesel engine. Proceedings of the Institution of Mechanical Engineers, Part D: Journal of Automobile Engineering, 2004. 218(1): p. 93-104.
22. Reeves, M., et al., Barrel swirl breakdown in sparkignition engines: insights from particle image velocimetry measurements. Proceedings of the Institution of Mechanical Engineers, Part D: Journal of Automobile Engineering, 1999. 213(6): p. 595-609.
23. Rizalman Mamat, et al. Effect of Air Intake Pressure Drop on Performance and Emissions of a Diesel Engine Operating with Biodiesel and Ultra Low Sulphur Diesel (ULSD). In International Conference on Renewable Energy and Power Quality (ICREPQ'09). 2009. Valencia, Spain.

24. Benajes J., et al., The effect of swirl on combustion and exhaust emissions in heavy-duty diesel engines. Proceedings of the Institution of Mechanical Engineers, Part D: Journal of Automobile Engineering, 2004. 218(10): p. 1141-1148.
25. Kim, K., et al., Investigation of the Swirl Effect on Diffusion Flame in a Direct-Injection (DI) Diesel Engine Using Image Processing Technology. Energy & Fuels, 2008. 22(6): p. 3687-3694.
26. Saad Idris, Bari, S., (2011). Effects of Guide Vane Swirl and Tumble Device (GVSTD) to the Air Flow of Naturally Aspirated CI Engine, in: Prof. Ali Mohammad (Ed.), International Conference on Mechanical Engineering 2011 (ICME2011). Progressive Printers Pvt. Ltd., Dhaka, Bangladesh.

Contact

Bhagyada Dhingra
Fiat-Chrysler Automotive pvt Ltd.
bhagyada.dhingra@fcagroup.com

Sparsh Sharma
Moscow Institute of Physics & Technology
sssparsh14@gmail.com

The Engineering Meetings Board has approved this paper for publication. It has successfully completed SAE's peer review process under the supervision of the session organizer. The process requires a minimum of three (3) reviews by industry experts.

ISSN 0148-7191

http://papers.sae.org/2015-26-0095